Article

PLK1-dependent phosphorylation restrains EBNA2 activity and lymphomagenesis in EBV-infected mice

Xiang Zhang[1] , Patrick Schuhmachers[2] , André Mourão[3,4], Piero Giansanti[5] , Anita Murer[2],
Sybille Thumann[1], Cornelia Kuklik-Roos[1], Sophie Beer[1] , Stefanie M Hauck[6] ,
Wolfgang Hammerschmidt[1] , Ralf Küppers[7] , Bernhard Kuster[5,8] , Monika Raab[9] ,
Klaus Strebhardt[9] , Michael Sattler[3,4,*] , Christian Münz[2,**] & Bettina Kempkes[1,***]

Abstract

While Epstein–Barr virus (EBV) establishes a life-long latent infection in apparently healthy human immunocompetent hosts, immunodeficient individuals are at particular risk to develop lymphoproliferative B-cell malignancies caused by EBV. A key EBV protein is the transcription factor EBV nuclear antigen 2 (EBNA2), which initiates B-cell proliferation. Here, we combine biochemical, cellular, and in vivo experiments demonstrating that the mitotic polo-like kinase 1 (PLK1) binds to EBNA2, phosphorylates its transactivation domain, and thereby inhibits its biological activity. EBNA2 mutants that impair PLK1 binding or prevent EBNA2 phosphorylation are gain-of-function mutants. They exhibit enhanced transactivation capacities, accelerate the proliferation of infected B cells, and promote the development of monoclonal B-cell lymphomas in infected mice. Thus, PLK1 coordinates the activity of EBNA2 to attenuate the risk of tumor incidences in favor of the establishment of latency in the infected but healthy host.

Introduction

Epstein–Barr virus (EBV) is associated with multiple malignancies including B-cell lymphomas and B-cell lymphoproliferative diseases (Longnecker *et al*, 2013; Farrell, 2019; Shannon-Lowe & Rickinson, 2019). More than 90% of the world population are infected with EBV. Based on an intimate virus–host interaction, the virus establishes a latent infection in resting memory B cells (Thorley-Lawson & Gross, 2004). Infected B cells are activated, enter the cell cycle, and proliferate and maintain the viral circular genomes in a process that is strictly coordinated with the cell cycle of the host cell. While entering the memory B-cell compartment, viral gene expression is gradually silenced to evade host immune surveillance. Reactivation of viral replication and virus production occurs occasionally (Munz, 2019).

EBV nuclear antigen 2 (EBNA2) is a key transcription factor that initiates and maintains the expression of viral and cellular target genes which are critical for the growth transformation of B cells by EBV (Kempkes & Ling, 2015; West, 2017). EBNA2 can activate the transcription of the viral latent membrane protein 1 (LMP1) and the cellular Myc gene in the absence of de novo protein synthesis. Thus, both are direct target genes of EBNA2 (Kaiser *et al*, 1999). Both proteins can induce an avalanche of secondary EBNA2 target genes. LMP1 promotes proliferation and cell survival. This multifunctional membrane oncoprotein activates the cellular NFκB, JNK, and STAT signaling cues and thereby mimics CD40 signaling (Thorley-Lawson, 2001). The proto-oncoprotein and transcription factor MYC stimulate global RNA and protein synthesis to foster cell growth of quiescent lymphocytes and cell cycle progression in normal non-malignant cells. High-level MYC expression is associated with

1 Research Unit Gene Vectors, Helmholtz Zentrum München, German Research Center for Environmental Health, München, Germany
2 Viral Immunbiology, Institute of Experimental Immunology, University of Zürich, Zürich, Switzerland
3 Institute of Structural Biology, Helmholtz Zentrum München, German Research Center for Environmental Health, Neuherberg, Germany
4 Department of Chemistry, Bavarian NMR Center, Technical University of Munich, Garching, Germany
5 Chair of Proteomics and Bioanalytics, Technical University of Munich, Freising, Germany
6 Research Unit Protein Science and Metabolomics and Proteomics Core Facility, Helmholtz Zentrum München, German Research Center for Environmental Health, München, Germany
7 Institute of Cell Biology (Cancer Research), University Hospital Essen, Essen, Germany
8 Bavarian Center for Biomolecular Mass Spectrometry, Technical University of Munich, Freising, Germany
9 Department of Gynecology and Obstetrics, Johann Wolfgang Goethe University, Frankfurt am Main, Germany
   *Corresponding author. Tel: +49 89 289 13867; E-mail: sattler@helmholtz-muenchen.de
   **Corresponding author. Tel: +41 44 635 3716; E-mail: muenzc@immunology.uzh.ch
   ***Corresponding author. Tel: +49 8931871354; E-mail: kempkes@helmholtz-muenchen.de

lymphomagenesis, but in the absence of co-stimulatory signals, it may also induce apoptosis (Baluapuri *et al*, 2020).

In the nucleus, EBNA2 associates with cellular proteins to execute its function. The B-cell-specific transcription factor EBF1 (Friberg *et al*, 2015; Lu *et al*, 2016; Glaser *et al*, 2017) and CBF1/RBPJ, the major downstream effector of NOTCH signaling, serve as DNA anchors for EBNA2 (Henkel *et al*, 1994; Hsieh & Hayward, 1995; Ling & Hayward, 1995; Farrell *et al*, 2004). The C-terminal acidic transactivation domain (TAD) of EBNA2 recruits components of the pre-initiation complex and histone acetylases and also contributes to ATP-dependent chromatin remodeling by interacting with hSNF5/Ini (Cohen & Kieff, 1991; Cohen *et al*, 1991; Cohen, 1992; Tong *et al*, 1995a, 1995b, 1995c; Wang *et al*, 2000; Kwiatkowski *et al*, 2004). The TAD of EBNA2 is intrinsically unstructured. In complex with the histone acetylase CBP or the TFIIH subunit Tfb1, a 9-residue amphipathic α-helix within this TAD is formed (Chabot *et al*, 2014). Cellular proteins may control EBNA2 transcriptional activities by protein–protein interactions or modification. The MYND domain of the repressor BS69 can bind as a dimer to the EBNA2 TAD and its flanking regions and attenuates EBNA2 activity as well as transformation efficiency (Harter *et al*, 2016; Ponnusamy *et al*, 2019).

In search for additional cellular factors controlling EBNA2 function, we have performed a label-free mass spectrometry-based quantification of cellular proteins in EBNA2 immunoprecipitates and found polo-like kinase 1 (PLK1). PLK1 is a serine/threonine–protein kinase that controls G2/M transition and progress through mitosis and cytokinesis in a tightly controlled order to secure genomic stability of the dividing cell. Through phosphorylation of specific substrates, PLK1 promotes activation of the mitotic driver Cyclin B1/CDK1 in the late G2-phase, triggering prophase onset (Nakajima *et al*, 2003; Watanabe *et al*, 2005; Gheghiani *et al*, 2017). PLK1 recognizes its substrates by a conserved C-terminal polo-box domain (PBD). Frequently, PBD binds to pre-phosphorylated epitopes generated by the mitotic CDK1 kinase or other proline-directed kinases such as MAPK (Elia *et al*, 2003a, 2003b; Lowery *et al*, 2005). This process is referred to as non-self-priming (Barr *et al*, 2004; Lee *et al*, 2014). Since primary tumors from various tissues express elevated levels of PLK1, and this high-level expression frequently correlates with a poor prognosis (Wolf *et al*, 1997), PLK1 is a potential oncotarget for molecular cancer therapy and a prognostic marker (Yuan *et al*, 1997; Rodel *et al*, 2020; Rosenblum *et al*, 2020). Preclinical and clinical studies currently test potential further clinical indications for small molecule or siRNA-based PLK1 inhibitors (Liu *et al*, 2017). However, there is now increasing evidence that PLK1 can also act as a tumor suppressor when expressed in the context of specific tumor types. Thus, there is a strong need to characterize and define the exact molecular features of tumors that may be treated with PLK1 inhibitors (de Carcer, 2019).

Here, we show that PLK1 directly binds to EBNA2. EBNA2/PLK1 complex formation is strongly enforced by EBNA2 residue S379 phosphorylation catalyzed by the mitotic Cyclin B/CDK1 complex. PLK1 phosphorylates the C-terminal transactivation domain of EBNA2 and attenuates its activity. EBNA2 mutants that lack either the main PLK1 docking site or the two phosphorylation sites are gain-of-function mutants that promote lymphoma incidence in EBV-infected humanized mice. This indicates that PLK1 acts as a tumor suppressor in EBV-driven carcinogenesis.

Results

Cyclin B/CDK1 primes EBNA2 residue S379 for polo-like kinase 1 (PLK1) binding

To identify potential EBNA2 interacting cellular proteins, we transfected EBV-negative DG75 B cells with HA-tagged EBNA2 expression constructs or the corresponding HA-expression vector and performed immunoprecipitations with HA-specific antibodies. Tryptic peptides of these immunoprecipitates were analyzed and quantified by label-free mass spectrometry. Polo-like kinase 1 (PLK1) was one of 19 proteins that were significantly enriched in EBNA2 co-immunoprecipitates (Table EV1). As expected, the EBNA2 DNA anchor protein CBF1/RBPJ was one of these proteins, demonstrating that the experimental approach was valid. Importantly, PLK1 and EBNA2 specifically co-immunoprecipitated from whole cell extracts of EBV-infected B cells in which both proteins are expressed at endogenous physiological levels (Fig 1).

To identify PLK1 docking sites within EBNA2, EBNA2 deletion fragments were generated and tested for binding to PLK1 by transfection and co-immunoprecipitation (Fig 2A–C). The smallest EBNA2 fragment that efficiently bound PLK1 mapped to region 342–474. Sub-fragments of either 327–487 or 342–474 showed some residual binding, but none of these regions conferred binding efficiencies similar to the precursor.

PLK1 frequently binds to phosphorylated substrates that are primed by cellular kinases like Cyclin B/CDK1. These substrates share a consensus motif [Pro/Phe]-[Φ/Pro]-[Φ]-[Thr/Gln/His/Met]-Ser-[pThr/pSer]-[Pro/X] (Φ represents hydrophobic and X represents any residue) specific for binding to the Polo-box binding domain (PBD) of PLK1 (Elia *et al*, 2003a). Crystal structures of the PLK1 PBD in complex with peptides demonstrate how the positively charged groove of PBD docks onto negatively charged phosphopeptides of diverse substrates. EBNA2 exhibits three potential Cyclin B/CDK1 phosphorylation and PBD docking sites located at residue T267, S379, and S470 (Fig 2D). Mutants involving the respective residues were tested for PLK1 binding by transfection and co-precipitation. The mutation TSS377VAA impaired PLK1 binding dramatically while all other EBNA2 mutations did not affect PLK1 binding (Fig 2E). To specify the contribution of EBNA2 residue S379 phosphorylation, a heptapeptide (PNTSSPS) and phospho-
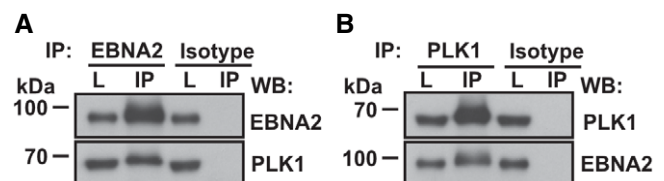

Figure 1. EBNA2 and PLK1 complexes in EBV-infected B-cell lines.

A, B Co-immunoprecipitation (IP) of EBNA2 (A) and PLK1 (B) using EBNA2-, PLK1-specific antibodies, or isotype-matched control antibodies performed on total cell lysates (L) of lymphoblastoid long-term B-cell cultures (LCLs) infected with recombinant EBV strain 2089, which is based on EBV strain B95-8 (Delecluse *et al*, 1998).

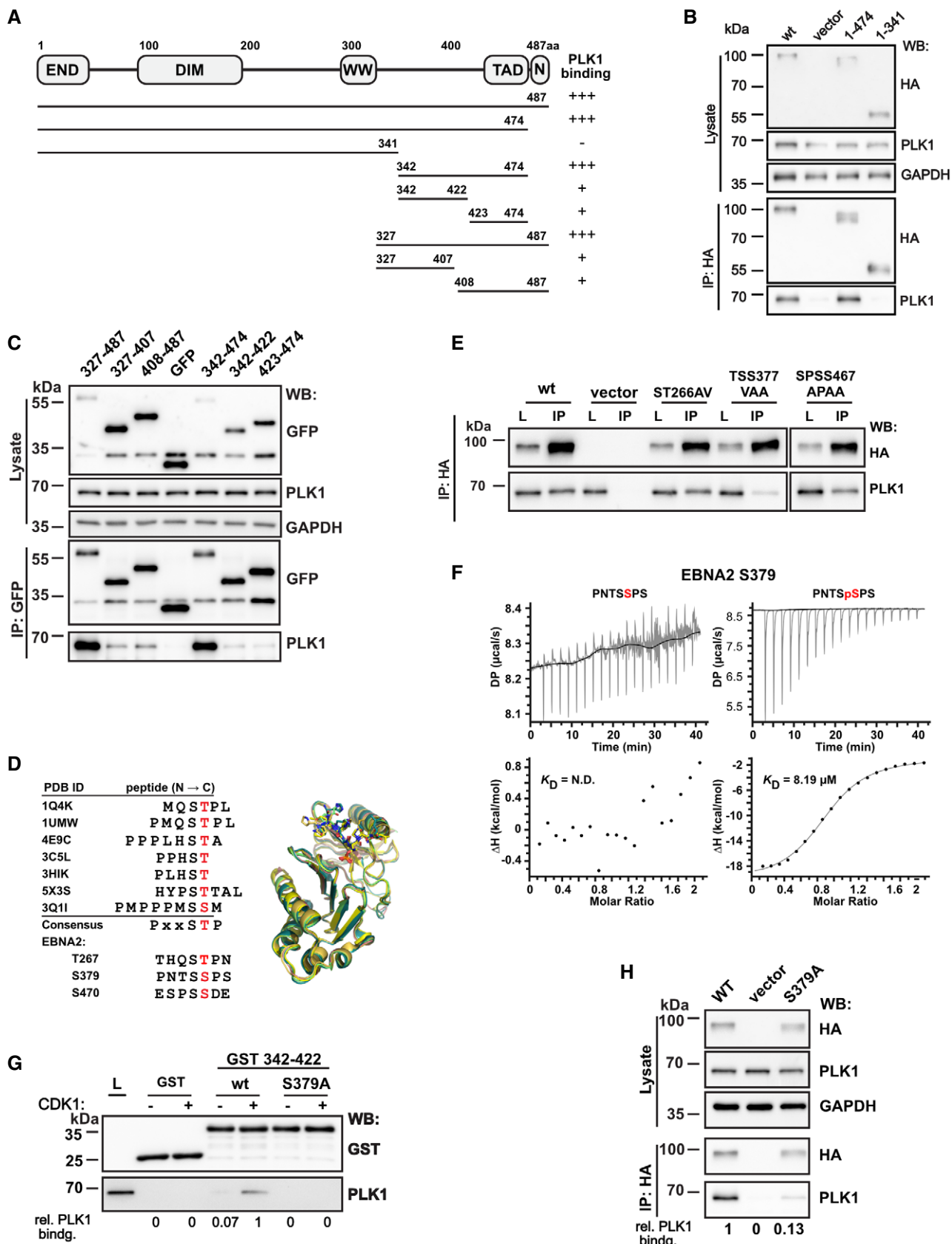Source data are available online for this figure.

Figure 2.

heptapeptide (PNTSpSPS) were tested for PBD (PLK1 residue 345-603) binding by isothermal titration calorimetry (ITC). The phosphorylated peptide bound PBD in a molar ratio of 1:1 whereas no interaction was detected using the unmodified peptide. The PNTSpSPS/PBD interaction is micromolar with a dissociation constant of $K_D = 8.19$ μM (Fig 2F). GST-EBNA2 342–422 expressed and purified from bacterial extracts did hardly pulldown any PLK1 from cellular extracts. Phosphorylation of the EBNA2 protein produced in bacteria by Cyclin B/CDK1, an enzyme not present in bacteria, strongly enhanced PLK1 binding. EBNA2 (342–422) S379A mutant did not bind PLK1, and phosphorylation by Cyclin B/CDK1 could not reconstitute binding (Fig 2G). Also, as shown by transfection, EBNA2 S379A binding to PLK1 was severely impaired (Fig 2H). We conclude that EBNA2 residue S379 is a PLK1 docking site primed by Cyclin B/CDK1 phosphorylation.

The C-terminus of EBNA2 is the substrate of PLK1

In order to test whether EBNA2 is phosphorylated by PLK1, EBNA2/PLK1 complexes were co-precipitated from cellular extracts of DG75 cells induced with doxycycline to express HA-EBNA2 (DG75[Dox HA-EBNA2]) (Fig 3A). The precipitates were submitted to kinase assays either in the presence or absence of exogenous recombinant PLK1. Phosphorylation of EBNA2 was readily detected in the co-precipitates and was enhanced by the addition of exogenous recombinant PLK1 to the co-precipitates (Fig 3B). EBNA2 phosphorylation was prevented upon addition of Volasertib, a PLK1-specific inhibitor, to the co-precipitates of EBNA2 and endogenous PLK1 (Fig 3C), corroborating the evidence that the endogenous PLK1 trapped in the co-precipitate is the active kinase.

To identify the amino acid residues that are phosphorylated by PLK1, bacterially expressed EBNA2 was phosphorylated by active recombinant PLK1 or left untreated. The EBNA2 protein was digested by trypsin and endoproteinase GluC (V8 Protease) in parallel. Tryptic or V8 protease-derived peptides and phosphopeptides were identified by mass spectrometry (MS). Since neither tryptic- nor V8-derived peptide covered the C-terminus of EBNA2 sufficiently, a subfragment (453–474) of EBNA2 flanked by arginine residues and expressed as a GST fusion protein was used for further tryptic digest and phosphopeptide mapping (Fig EV1). Initially, 11 potential phosphorylation sites were found. Of these, five phosphorylation sites (S184, 258, 457, 479, and T465) were confidently

localized (Fig EV2) and six additional sites (T175, 178, 263, 267, 464, and S266) were mapped ambiguously with less confidence. The alignment (Fig EV3) of the protein sequence of different EBV type 1 or type 2 strains or related non-human primate lymphocryptoviruses (LCV) revealed that residues S184 and S258 were conserved in type 1 EBV strains, and S379 and S479 were identical across species while S457 was conserved across human sequences. T465 was identical across human sequences and replaced by the similar T residue in LCV.

To test, if the five confidently localized phosphorylation sites identified in vitro are relevant also in cells, EBNA2 mutants with a singular or combined mutations were generated and expressed in DG75 B cells. Immunoprecipitations and subsequent kinase assays based on endogenous PLK1 trapped in the precipitates were performed (Fig 3D). None of the mutations severely impaired PLK1 binding but Volasertib prevented phosphorylation of all EBNA2 proteins. In the absence of Volasertib, phosphorylation of S184A was slightly reduced, while phosphorylation of S258A and S479A was not reduced. Phosphorylation of the EBNA2 mutants S457A and T465V was severely impaired, and the combination of both mutations (S457A/T465V) abolished phosphorylation (Fig 3E). To corroborate this finding, GST-EBNA2 246-487 either in wild-type or as S457A/T465V mutant was submitted to kinase assays using recombinant PLK1 in vitro. This experiment resulted in efficient phosphorylation of wild-type but not mutant EBNA2 S457A/T465V (Fig 3F). We conclude that the PLK1 docking and the PLK1 phosphorylation site are two independent EBNA2 modules that can be dissected and analyzed by specific mutations (Fig 3G).

To test the phosphorylation mutants for their biological activity, we used a luciferase reporter construct driven by an EBNA2 responsive artificial promoter that harbors a multimerized CBF1 binding site to recruit EBNA2 (Minoguchi *et al*, 1997). All mutants that carried either the S457A, the T465V mutation, or both mutations showed enhanced transactivation potential, suggesting that PLK1 might negatively regulate EBNA2 activity (Fig 3H). Since the C-TAD of EBNA2 is known to bind the histone acetylase and co-activator p300 (Chabot *et al*, 2014), p300 binding to EBNA2 phosphorylation mutants was tested by GST-pulldown experiments. While p300 binding of the single EBNA2 phosphorylation mutants was strongly enhanced by approximately 2- to 3-fold, binding by the double-mutant S457A/T465V was increased even 8- to 9-fold. Thus, enhanced p300 binding of EBNA2 phosphorylation mutants

correlates well with improved transactivation activity. This finding suggests that PLK1 phosphorylation hinders p300 recruitment to EBNA2, thereby inhibiting EBNA2 transactivation (Fig 3I).

To directly study whether PLK1 inhibits EBNA2 functions, PLK1 and EBNA2 were co-expressed and luciferase reporter assays were performed (Fig 4A). In these transient transfection experiments, all EBNA2 mutants and all PLK1 mutants were expressed well (Fig 4B).

EBNA2 wt activity was significantly reduced by co-expression of PLK1 but not affected by the kinase-dead K82M PLK1 mutant. The activity of the docking site mutant S379A was weakly impaired by co-expression of PLK1, suggesting that residual binding activity that is evident in Fig 2H (last lane) might still recruit PLK1 activity. Importantly, the transactivation capacity of the phosphorylation mutant S457A/T465V was not affected by PLK1 co-expression,
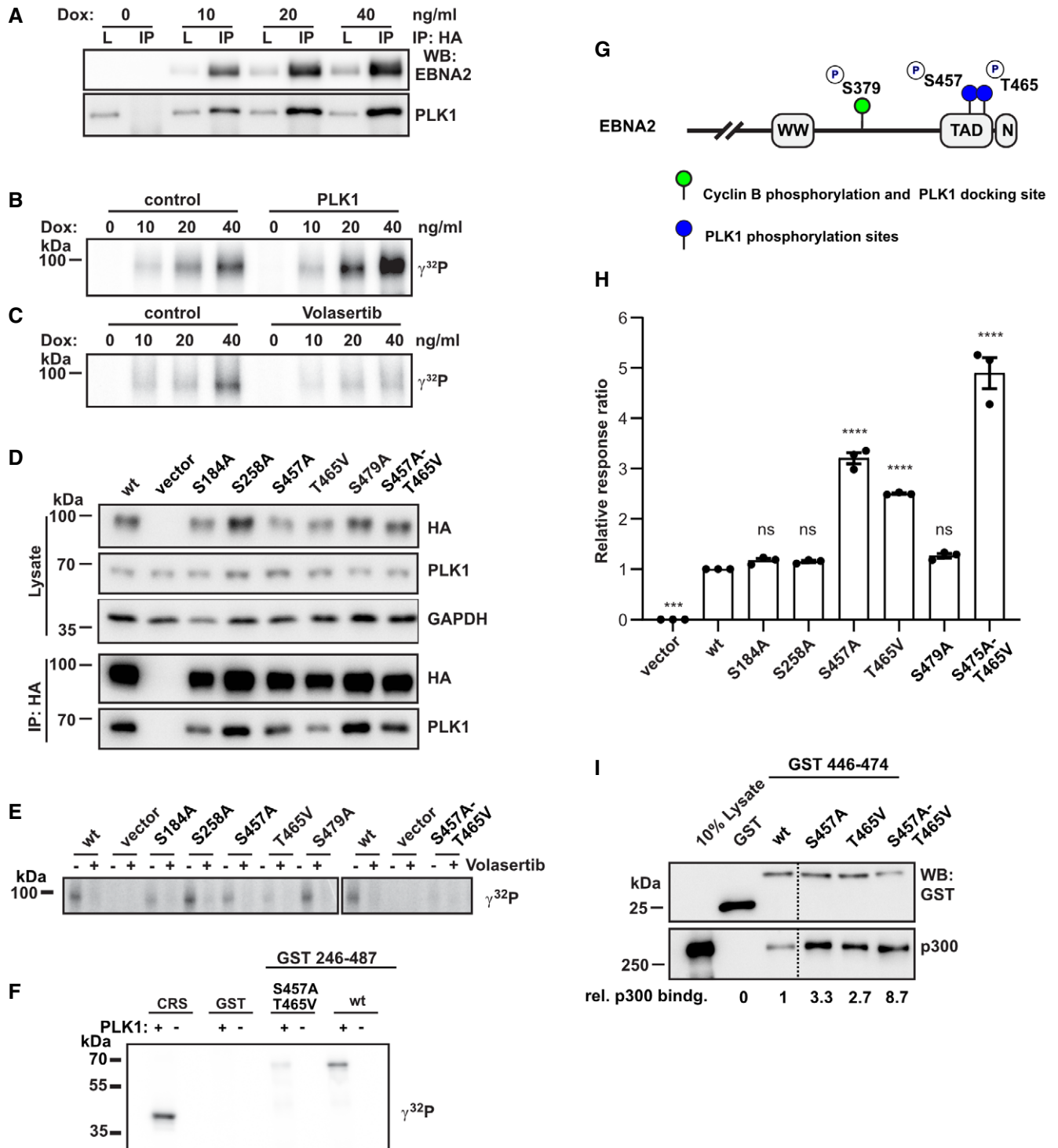

Figure 3.

Figure 3. PLK1 phosphorylates the EBNA2 residue S457 and T465 within the C-terminal transactivation domain.

A Doxycycline (Dox) induction of EBNA2 in DG75[Dox HA-EBNA2] cells treated for 24 h. Co-immunoprecipitates of HA-EBNA2 and endogenous PLK1 are visualized by Western blotting.
B EBNA2/PLK1 co-precipitates were submitted to kinase reactions using [γ-^{32}P] ATP in the absence (control) or presence of 50 ng recombinant active PLK1.
C EBNA2 co-precipitates were submitted to kinase reactions in the absence (control) or the presence of the PLK1 inhibitor Volasertib (40 nM).
D EBNA2 candidate phosphorylation mutants were expressed in DG75 B cells and tested for PLK1 binding by co-immunoprecipitations followed by Western blotting.
E Immunoprecipitates were submitted to kinase reactions as in B, but samples were treated with Volasertib (40 nM) (+) or treated with solvent only (−).
F GST-EBNA2 fragment 246–487 wt and mutant S457A/T465V were treated with recombinant active PLK1 (+) in the presence of [γ-^{32}P] ATP in vitro or left untreated (−). CRS, an artificial PLK1 test substrate (Yuan *et al*, 2002), was used as a positive control.
G Schematic presentation of EBNA2 phosphorylation sites by CDK1 and PLK1.
H HA-tagged EBNA2 candidate phosphorylation mutants were expressed in DG75 B cells and tested for activation of an EBNA2/CBF1 responsive promoter reporter luciferase plasmid. Activation of the reporter gene is shown as relative response ratio normalized to Renilla luciferase activity and shown relative to wt activity. Data were presented as the mean ± SEM of *n* = 3 biological replicates. Statistical significance was tested by one-way ANOVA followed by Tukey's multiple comparison test (ns: not significant, ***$P < 0.001$, ****$P < 0.0001$, vs WT).
I GST-pulldown assay using GST-EBNA2 446-474 as a bait to purify cellular proteins from DG75 cells followed by Western blotting and quantification of signals obtained by GST- and p300-specific antibodies. Relative binding affinities (rel. p300 bindg.) are normalized to the wt signal. Since 3 lanes of the original blot were excised a broken line marks the borders between two parts in the figure.

Source data are available online for this figure.

demonstrating that EBNA2 S457A/T465V is resistant to PLK1 treatment. Since the kinase-dead PLK1 mutant did not impair the transactivation capacity of any EBNA2 protein, we conclude that PLK1 binding is necessary but not sufficient to inhibit EBNA2 and the phosphorylation of EBNA2 by PLK1 is required to inhibit EBNA2.

In summary, PLK1 phosphorylates S457 and T465 within the TAD of EBNA2 to attenuate its activity and to impair p300 binding. PLK1 uses S379A as a phosphorylation-dependent docking site that can be primed by Cyclin B/CDK1.

EBV strains expressing EBNA2 mutants deficient for PLK1 docking or phosphorylation are gain-of-function mutants in B-cell immortalization assays

To test EBNA2 mutants defective for PLK1 binding or phosphorylation by PLK1 for their B-cell immortalization potential, three new viral mutants based on the viral backbone of the recombinant EBV strain p6008 (Mrozek-Gorska *et al*, 2019; Pich *et al*, 2019) were generated. Carboxyl-terminally HA-tagged EBNA2 (EBV wt), HA-tagged EBNA2 S379A (EBV S379A), and HA-tagged EBNA2 S457A/T468V (EBV S457A/T465V) were inserted into the backbone of the recombinant EBV strain p6008 by homologous recombination using a two-step positive-negative selection protocol, also called recombineering (Wang *et al*, 2009). The integrity of the viral genomes was controlled by restriction digest and sequencing (Fig EV4A–D). Infectious viruses were produced in HEK293 cells. Primary B cells from three unrelated donors were infected. During the first 6 days post-infection, the proliferation rates of EBV wt, EBV S457A/T465V, or EBV S379A-infected B cells were determined. The phosphorylation mutant S457A/T465V proliferated the fastest, followed by S379A- and wt-infected cells (Figs 5A and EV4E and F). Also, long-term cultures infected with EBV wt and both mutants could be established. The proliferation of these lymphoblastoid cell lines (LCLs) was characterized by counting the cells daily (Fig 5B). The proliferation rates of both long-term cultures infected with mutant viruses were higher than EBV wt-infected cells. EBNA2 expression levels in these long-term cultures were similar for wt and S379A but less pronounced for the S457A/T465V mutant.

LMP1 expression varied between the cell lines obtained from different donors but was consistently elevated in EBV S457A/T465V-infected cell lines compared with S379A and EBV wt-infected B cells. MYC expression was seen in all infected cultures, but MYC levels were not affected by individual virus variants indicating that MYC was not the driving force for the accelerated proliferation of the established LCLs (Fig 5C). In summary, both mutants were gain-of-function mutants with respect to proliferative capacities of the infected cell cultures and LMP1 activation. In comparison, these features were more pronounced in EBV S457A/T465V than in S379A-infected B cells.

Enhanced frequencies of B-cell lymphomas in humanized mice infected with EBV S379A or EBV S457A/T465V

Since EBV does not infect murine B cells, tumor development and immune control were studied in humanized mice. Immunodeficient NSG (NOD scid $\gamma_c^{-/-}$) mice can be engrafted with CD34^{+} human hematopoietic progenitor cells to develop human immune system components that can be readily infected with human lymphotropic pathogens, including EBV. These chimeric humanized mice were used previously to study EBV-induced tumor formation after EBV infection and anti-viral immune mechanisms against EBV in vivo (Strowig *et al*, 2009). Hence, we infected three cohorts (designated experiments 1, 2, and 3) of humanized mice intraperitoneally with 10[5] Green Raji Units (GRU) of EBV and analyzed viral blood loads, CD8^{+} and CD4^{+} T-cell composition as well as activation in their blood in weekly intervals. Five weeks post-infection, all EBV-positive mice were sacrificed to analyze tumor development (Fig 6A). In two out of three independent experiments, infection with EBV S457A/T465V caused increased mortality rates compared with EBV wt- or S379A-infected animals (66% survival in the second and 20% in the third experiment; Fig 6B). In addition, mice that were infected with either of the two EBV mutants presented with higher incidence of tumor development in spleen, peritoneal cavity, or lymph nodes (23% for WT, 36% for S379A, and 44% for S457A/T465V; Fig 6C). Viral loads in the spleen of mice infected with mutants were slightly elevated 5 weeks post-infection when mice were sacrificed (Fig 6D). In blood, viral loads of EBV wt- and EBV S379A-infected mice gradually increased until week 3 and remained at similar levels until the end of the experiment. In contrast, viral loads in mice within the EBV S457A/T465V mutant group reached higher levels already 2 weeks after infection and started to decrease at 4 weeks post-infection (Fig 6E).
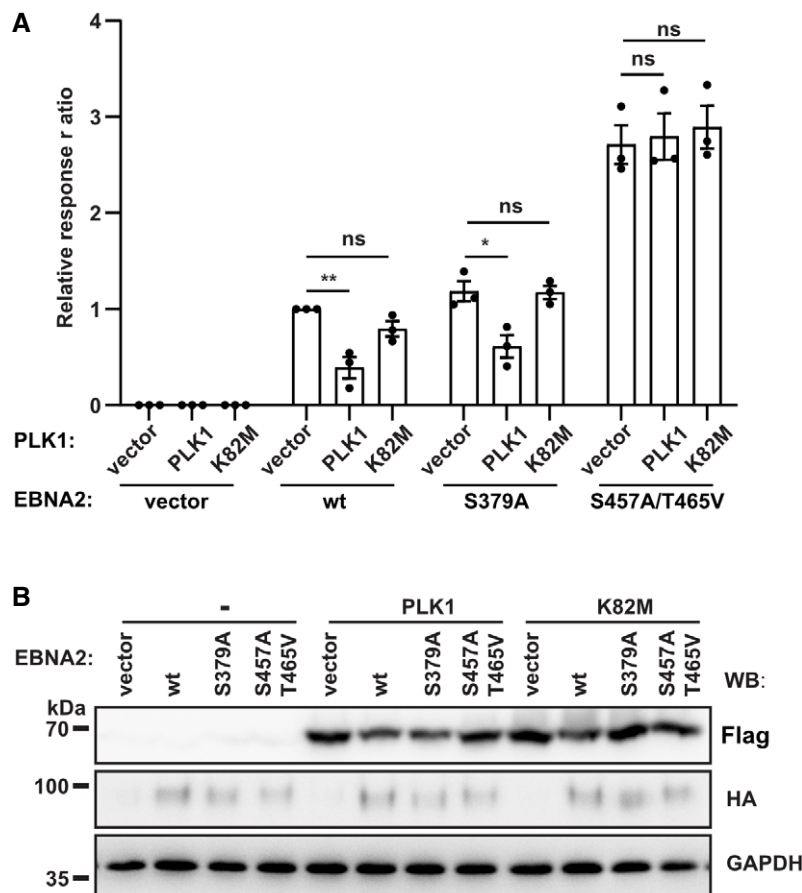
Figure 4. PLK1 inhibits EBNA2 activity by phosphorylating residues S457/T465.

A Flag-tagged active (PLK1) and kinase inactive PLK1 (K82 M) were co-expressed with HA-EBNA2 wt, docking site mutant (S379A) and phosphorylation mutant (S457A/T465V) and tested for activation of an EBNA2/CBF1 responsive promoter reporter in DG75 cells. Activation of the reporter firefly luciferase gene is shown as relative response ratio normalized to Renilla luciferase activity and shown relative to EBNA2 wt activity. Data were presented as the mean $\pm$ SEM of $n = 3$ biological replicates. Statistical significance was tested by two-way ANOVA followed by Tukey's multiple comparison test (ns: not significant, $*P < 0.05$, $**P < 0.01$).

B 30 μg of cellular extracts that were produced for luciferase assays were tested for protein expression using Flag-, HA- and GAPDH-specific antibodies.

Source data are available online for this figure.

EBV infection of B cells is well known to elicit a strong T-cell response. In particular, extensive CD8^{+} T-cell expansion and activation in blood is a common trait marking EBV infection in humanized mice. It usually follows, with a delay of about a week, rising viral loads (Strowig *et al*, 2009; Chatterjee *et al*, 2019) and correlates with these (Caduff *et al*, 2020; Zdimerova *et al*, 2021). As CD8^{+} T cells expand more strongly than CD4^{+} T cells in response to EBV infection, a rising CD8^{+} to CD4^{+} T-cell ratio indicates the extensive proliferation of CD8^{+} T cells.

Three weeks post-infection, the mean CD8^{+}/CD4^{+} T-cell ratios in mice infected with EBV S457A/T465V (0.99) were significantly higher than in EBV wt (0.37)-infected mice, while CD8^{+}/CD4^{+} T-cell ratios of EBV wt-infected animals increased later, at 4 weeks post-infection (Fig 6F).

CD8^{+} and CD4^{+} T-cell populations of mice infected with mutant virus started to expand already 2 weeks post-infection (Fig EV5A and B). Also, the relative fraction of CD8^{+} T cells expressing the activation marker HLA-DR increased from week 2 post-infection,

thus earlier than the control EBV wt-infected group (Fig EV5C and D). A similar trend could be observed for mice infected with the EBNA2 S379A mutant. Interestingly, the EBV S457A/T465V mutant more strongly induced the activation of CD4^{+} T cells in the blood of mice within 5 weeks of infection compared with the EBV wt-infected group (Fig EV5D). In contrast to blood, the fractions of CD8^{+} and CD4^{+} T cells in the spleen of infected animals did not differ between the groups (Fig EV4E) but a higher fraction of CD8^{+} and a significantly increased fraction of CD4^{+} T cells were HLA-DR-positive and thus activated in EBV S457A/T465V-infected animals (Fig EV4F and G). The development of memory T cells, i.e., effector memory (Tem), central memory (Tcm), or terminally differentiated subsets that re-express CD45RA (Temra), however, was not influenced by EBNA2 mutations (Fig EV5H and I). In summary, EBV S379A and EBV S457A/T465V infections developed more rapidly in humanized mice, resulting in earlier immune responses, increased lymphomagenesis and more frequent demise of the mice.

Tumors of EBV S379A- or EBV S457A/T465V-infected mice frequently present as monoclonal B-cell lymphomas

The diversity of immunoglobulin gene rearrangements and sequences can be used to define the clonal composition of a given B-cell population (Kuppers *et al*, 1993; Rajewsky, 1996). In experiment 2, 1 out of 5 EBV wt, 2 out of 4 EBV S379A, and 2 out of 4 EBV S457A/T465V-infected mice developed tumors. The clonality of macroscopically visible tumors detected in experiment 2 was assessed by PCR of rearranged IgH V genes, using subgroup-specific
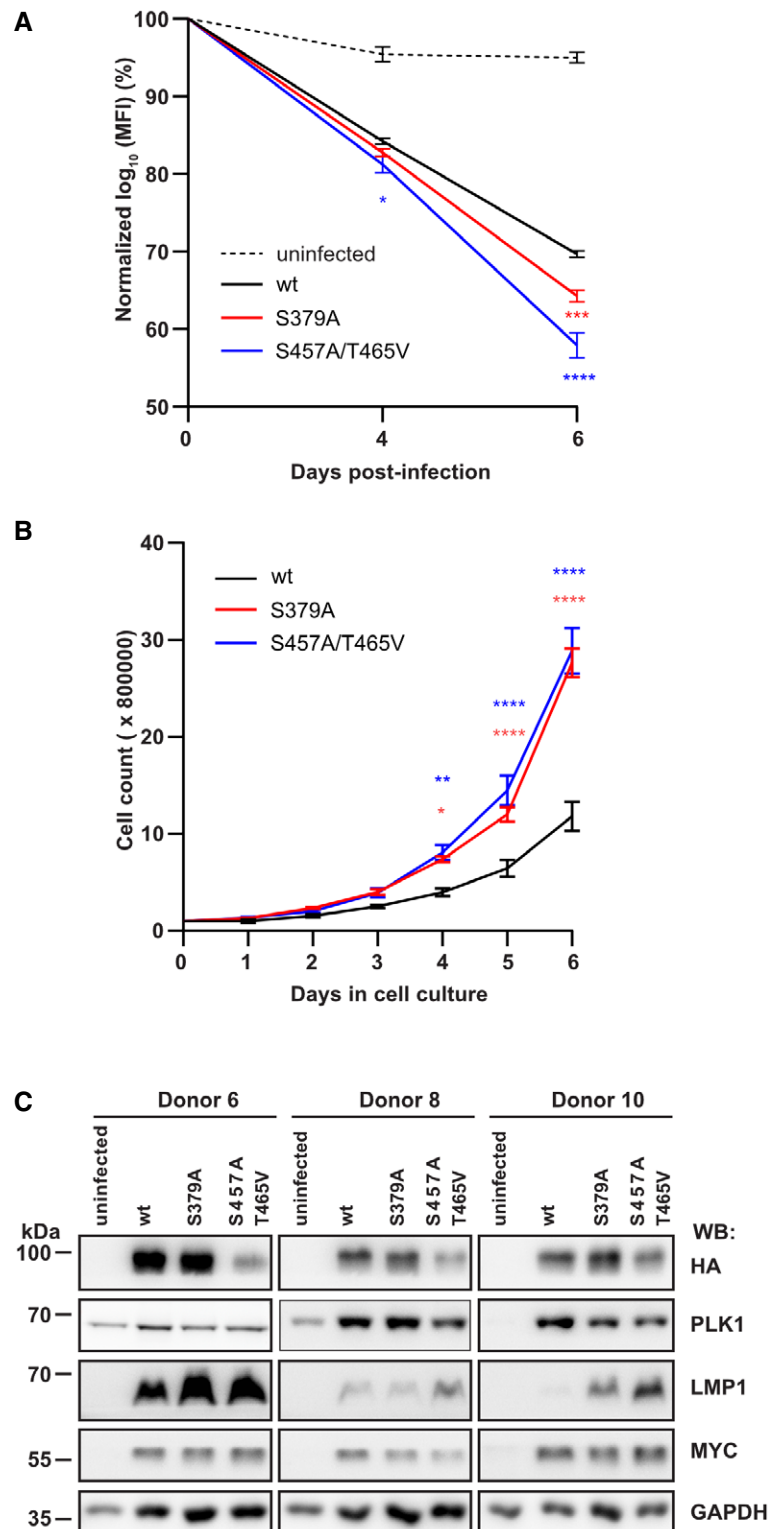

Figure 5.

◀

Figure 5.   EBV strains expressing EBNA2 mutants deficient for PLK1 docking or phosphorylation accelerate B-cell proliferation and express elevated levels of the viral LMP1 protein.

A   Primary B cells were stained with cell trace violet before they were infected, and cell cultures were started. Loss of the fluorescent cell tracking dye was recorded by flow cytometry to monitor proliferation on days 0, 4 and 6 post-infection. Mean values for three biological replicates, standard deviation, and significance of changes in signal loss of mutants compared with wild-type controls Data were presented as the mean ± SEM of $n = 3$ biological replicates. Statistical significance was tested by two-way ANOVA followed by Tukey's multiple comparison test (*$P < 0.05$, ***$P < 0.001$, ****$P < 0.0001$, vs WT).

B   Long-term growth-transformed B-cell cultures infected with recombinant EBV mutants were seeded at a starting concentration of 2×10^5 cells per ml. Data were presented as the mean ± SEM of $n = 4$ biological replicates. Statistical significance was tested by two-way ANOVA followed by Tukey's multiple comparison test (*$P < 0.05$, **$P < 0.01$, ****$P < 0.0001$, vs WT).

C   Expression of EBNA2, LMP1, PLK1, MYC, and GAPDH was analyzed by Western blotting and immunostaining of whole cell extracts of cell lines established from 3 individual donors.

Source data are available online for this figure.

IgH V primers together with an IgH J primer mix in separate reactions, followed by Sanger sequencing of amplificates obtained (Table EV2). Polyclonal B-cell expansions were found in the splenic tumors of EBV wt (#13) and in one splenic tumor of EBV S379A (#23). In all of the four analyzed tumor-bearing mice infected with mutant EBV, monoclonal B-cell populations were identified, sometimes on a background of remaining polyclonal B cells. In mouse #23, the spleen harbored a polyclonal B-cell population, while the peritoneum showed a monoclonal B-cell expansion. This analysis validates that the tumors developing in EBNA2 mutant mice are indeed monoclonal, and hence bona fide malignant B-cell lymphomas. In all five monoclonal lymphomas, productive in-frame IgH V genes were obtained. Three of the samples showed additional out-of-frame rearrangements, which likely represent the second IgH alleles of the monoclonal lymphomas defined by the in-frame rearrangements. Since humanized NOD scid $\gamma_c^{-/-}$ mice in the experimental setup of our study cannot generate germinal centers, we did not expect somatic hypermutation to occur. Indeed, somatic mutations were not observed in any specimen.

Discussion

EBNA2 mutations, which impair PLK1 binding or prevent phosphorylation by PLK1, accelerate cellular proliferation and tumor formation

Our study demonstrates that PLK1 directly binds to the phosphorylated EBNA2 residue S379 and phosphorylates S457 and T465 located in the transactivation domain of EBNA2. S457A/T465V missense mutants can still bind to PLK1 but are not phosphorylated. The EBNA2 docking site S379A and EBNA2 S457A/T465V phosphorylation mutants, both show enhanced transactivation capacities with S457A/T465V being stronger than S379A. This enhanced potential might be caused in part by the elevated levels of histone acetylase and co-activator p300 that binds to the S457A/T465V mutant. However, p300 is not the only candidate molecule that binds to the EBNA2 N-terminal TAD. Since several cellular factors that trigger transcription initiation and chromatin remodeling interact with the TAD of EBNA2, these might directly or indirectly contribute to the phenotype of S457A/T465V. The alignment of EBV and LCV protein sequences revealed a high conservation of all three residues across EBV strains. S379 and T465 were conserved even across species. Considering that the respective mutants are gain of function, i.e., activated proteins, we

think that PLK1 contributes to the establishment of latency by attenuating EBNA2 activity.

Both EBV mutants, which expressed EBNA2 S379A or S457A/T465T, were fully immortalization competent and initiated long-term proliferating B-cell cultures with accelerated cell division rates and elevated induction of the EBNA2 target gene LMP1. The impact of both mutations was further studied in humanized mice susceptible to EBV infection. Blood samples of infected mice were analyzed weekly for viral loads and immune responses of $CD4^+$ and $CD8^+$ T-cell populations. Elevated viral loads and $CD4^+$ and $CD8^+$ T-cell activation in the blood of EBV S457A/T465V of infected mice preceded $CD8^+$ T-cell expansion. On the day of sacrifice, splenic EBV loads were slightly elevated in both EBNA2 mutants compared with EBV wt-infected animals. Based on earlier publications, increasing viral loads were expected to precede expansion and activation of EBV-specific $CD8^+$ T cells since antigen abundance stimulates $CD8^+$ T-cell responses (Strowig *et al*, 2009; Shultz *et al*, 2010). Irrespective of the early adaptive immune response to infection, more EBV mutant-infected mice developed lymphomas when compared to EBV wt infections. The accelerated proliferation rates that we observed in cell culture might contribute to tumor size in mice. The enhanced transcriptional activities of the EBNA2 mutants induce higher LMP1 levels, which is a critical viral oncogene in B-cell transformation and thus also might promote tumor formation in vivo. In addition, both EBNA2 mutants might also induce distinct viral and cellular RNAs, which promote tumor progression but still are to be identified.

Importantly, tumors detected in mice infected with mutant virus were predominantly monoclonal and were detected in the spleen as well as in the peritoneum and in lymph nodes. The elevated viral loads seen in mice infected with mutant EBV might increase tumor incidence by amplifying the number of infected B cells in these animals and thereby might initiate the lymphoproliferative disease at multiple sites but they do not explain disease progression to monoclonal B-cell lymphomas. It will be interesting to study whether lymphomas in lymph nodes or peritoneum are metastatic descendants of splenic tumors. The genetic or epigenetic processes driving the clonal evolution of single cells and giving rise to monoclonal tumors still need to be explored.

PLK1 restrains the growth transformation potential of EBNA2 to establish tumor-free survival of latently infected hosts

Both mutants independently target highly conserved amino acid residues (Fig EV3) but surprisingly are both gain-of-function
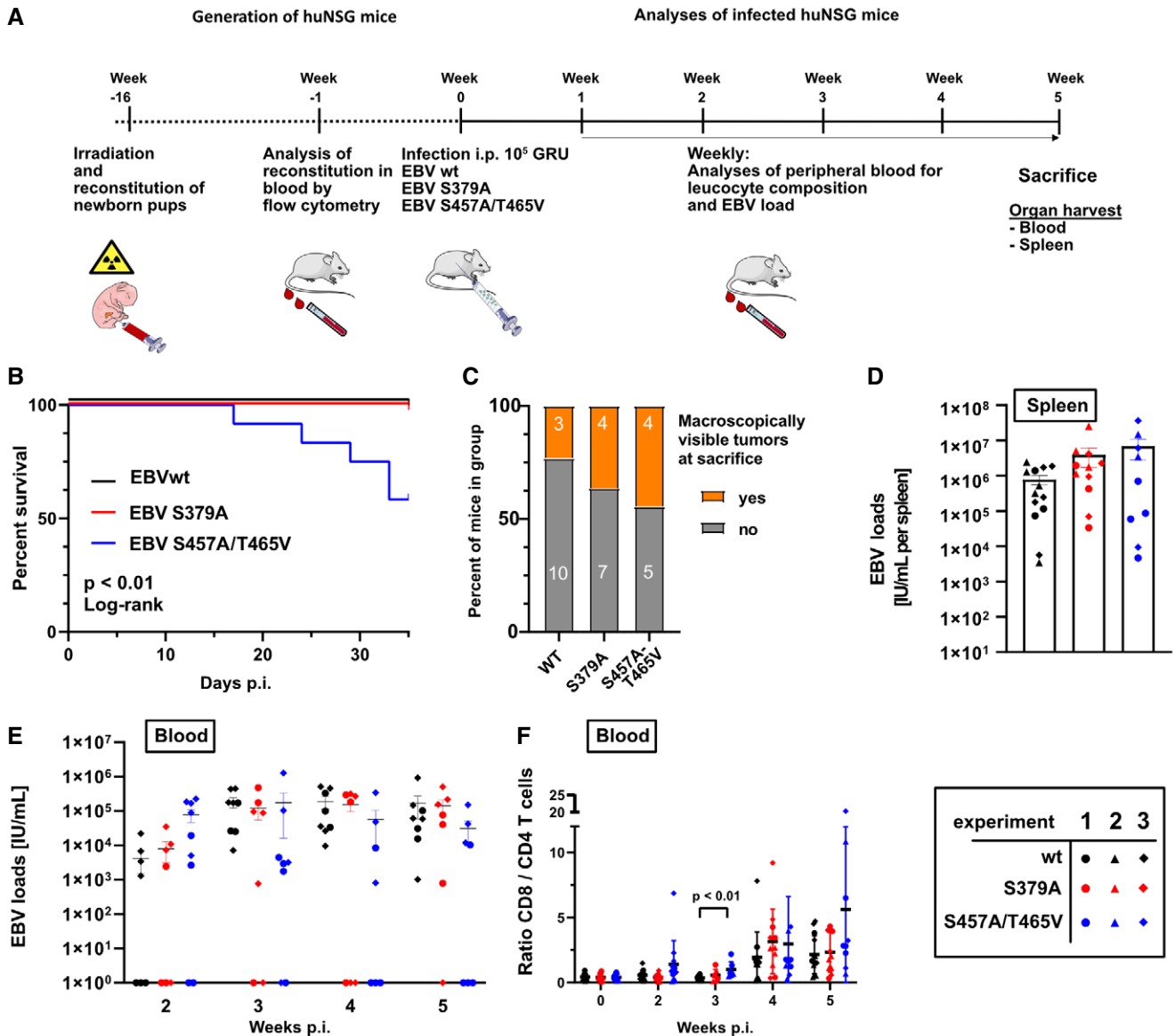
Figure 6. EBV strains carrying EBNA2 mutants with diminished PLK1 binding or resistant to PLK1 phosphorylation cause lymphomas in humanized mice more frequently than EBV wt.

A   Experimental setup (Images of animals, syringes, and blood collection tubes are derived from Servier Medical Art.).

B   Survival curve of humanized mice infected with 10^5 GRU EBV wt ($n = 13$), EBV S379A ($n = 11$), or EBV S457A/T465V EBV ($n = 9$). Log-rank test.

C   Percentage of mice having macroscopically visible tumors at the day of sacrifice. Numbers within bars indicate the total number of mice with or without tumors in the respective groups. Fisher's exact test.

D   Viral loads in spleen of infected humanized mice at the day of sacrifice. Error bars indicate mean ± SEM. Number of biological replicates per group: EBNA2 WT EBV: $n = 13$; EBNA2 S379A EBV: $n = 11$; EBNA2 S457A T465V EBV: $n = 9$.

E   Development of viral loads in blood of infected mice over a period of 5 weeks. Error bars indicate mean ± SEM. Number of biological replicates per group: EBNA2 WT EBV weeks 2–5: $n = 8$; EBNA2 S379A EBV weeks 2–5: $n = 7$; EBNA2 S457A T465V EBV week 2: $n = 9$, week 3: $n = 8$, week 4 and week 5: $n = 7$.

F   Flow-cytometric analyses of CD8$^+$/CD4$^+$ T-cell ratios in the blood of infected mice over a period of 5 weeks. Error bars indicate mean ± SD. Number of biological replicates per group: EBNA2 WT EBV weeks 0, 2, 4, and 5: $n = 13$; week 3: $n = 8$; EBNA2 S379A weeks 0, 2, 4, and 5: $n = 11$, week 3: $n = 7$; EBNA2 S457A T465V weeks 0 and 2: $n = 12$, week 3: $n = 7$, week 4: $n = 10$, week 5: $n = 9$.

Data information: The shape of data points indicates to which cohort (experiment 1, 2, or 3) the respective animal belongs while the color indicates the EBV EBNA2 mutant with which the animal was infected. Statistical significance was tested using the Mann–Whitney U-test with Holm–Sidak correction for multiple comparisons if not indicated differently.

mutants, which exhibit improved transformation capacities. We conclude that the control of EBNA2 activity is evolutionary conserved and might be beneficial for host and virus to protect

against cancerogenesis and establish and stabilize long-term latency and thus the viral reservoir in the host. Since PLK1 activity peaks in mitosis, PLK1 might restrain EBNA2 activities preferentially during

this time window. Unfortunately, since during mitosis the global cellular transcription of the condensed chromosomes and the viral episome is silenced, EBNA2 activity cannot be reliably tested in mitotic cells. There appears to be a strict biological necessity to dynamically control EBNA2 activity by multiple viral and cellular factors. Transient transfections and reporter gene studies have suggested that Cyclin B/CDK1 or the viral lytic kinase BGLF4 can control EBNA2 activity, but these studies have not linked their findings to PLK1 activity (Yue *et al*, 2004, 2005, 2006).

PLK1 is a key control element of multiple cell cycle stages including G2/M transition, M-phase progression, and cytokinesis. In addition, it has been shown before that PLK1 can affect the activity of cellular transcription factors through several mechanisms. Phosphorylation of the tumor suppressor p53 and the related p73 protein impair the transactivation activity of both transcription factors. In p73, the substrate site of PLK1 has been mapped to the TAD (Ando *et al*, 2004; Martin & Strebhardt, 2006; Koida *et al*, 2008; de Carcer, 2019). Phosphorylation of the transcription factor FOXO1 by PLK1 causes its nuclear exclusion and thereby prevents its action (Yuan *et al*, 2014). On the other hand, PLK1 phosphorylation of the transcription factor FoxM1, a critical transactivator of mitotic gene expression, induces FoxM1 activity (Marceau *et al*, 2019). It is tempting to speculate that PLK1 might contribute to the general mitotic transcriptional shut down by inhibiting distinct transcription factor activities. In parallel, PLK1 might guide the transcriptional activity of the cell to processes relevant to mitotic progression and maintenance of genomic integrity.

In healthy immunocompetent hosts, EBNA2 is expressed in a short time window immediately post-infection before either EBNA2 expression is silenced or the EBNA2 expressing cell is eliminated by the immune system. Immunodeficient patients, suffering from profound T-cell suppression, can develop aggressive EBNA2-positive B-cell lymphoproliferative diseases, and EBNA2 is a driving force for these tumor entities. The "primary goal" of latent viruses such as EBV is to establish a balanced equilibrium of its latent and lytic phase while tumor development is an accident in its life cycle with no benefit for virus dissemination (Shannon-Lowe & Rickinson, 2019). EBNA2 obeys the intracellular signaling cues that silence its activity during a short time window of the cell cycle in order to establish latency and maintain the viral life cycle rather than promoting tumorigenesis. It is well established that high-level expression of PLK1 promotes carcinogenesis in multiple tissues (Strebhardt & Ullrich, 2006; Strebhardt, 2010; Liu *et al*, 2017). PLK1 is also considered as an oncotarget for aggressive B-cell lymphomas since it stabilizes MYC (Ren *et al*, 2018). Currently, clinical trials evaluate the safety and efficacy of PLK1 inhibitors for patient treatment. However, in some tumor types high-level PLK1 expression can suppress cancerogenesis (Raab *et al*, 2018; de Carcer, 2019). Whether it exerts oncogenic or tumor suppressor functions depends on the cellular environment, defined by tissue origin, genetic lesions and potential additional factors that still need to be defined. Our study makes an important contribution to elucidate the bi-functional nature of PLK1 in its specific context.

Here, we show that PLK1 is an important cellular control factor that restrains the proliferation and transformation of latently EBV-infected B cells driven by a growth program that depends on EBNA2. Since two distinct EBNA2 mutants that both target independent PLK1-related functions of the EBNA2/PLK1 complex promote

cancerogenesis, we conclude that PLK1 might act as a tumor suppressor in EBNA2-driven lymphomagenesis. Until to date, the interaction of EBNA2 with PLK1 was unknown, and thus, latent EBV was not considered a risk factor in PLK1 inhibitor-based therapeutic strategies. Knowing that latent EBV is ubiquitously found in human hosts, PLK1 inhibitors could cause adverse effects with detrimental consequences for immune-deficient patients, which are prone to EBV-related cancerogenesis. Humanized mice infected with EBV or specific EBV mutants will serve as pre-clinical animal models to study the action of PLK1 inhibitors in the context of latent EBV infection.

Materials and Methods

Cell culture

EBV-infected long-term cultures (LCLs), DG75 cells (Ben-Bassat *et al*, 1977), DG75$^{\text{Dox HA-EBNA2}}$ (Glaser *et al*, 2017), Raji (Pulvertaft, 1964), and HEK293 cells were cultured in RPMI 1640 supplemented with 10% fetal bovine serum (FBS), 1% non-essential amino acids, 2 mM L-glutamine, 1 mM sodium pyruvate, 100 U/ml penicillin, 100 μg/ml streptomycin, 100 nM sodium selenite, and 50 μM α-thioglycerols at 37°C in 6% CO_2 atmosphere. Media for HEK293 cells transfected with recombinant EBV and DG75$^{\text{Dox HA-EBNA2}}$ contained 1 μg/ml puromycin.

Purification of human primary B cell and LCL establishment

Human primary B cells isolated from adenoid from routine adenoidectomy were obtained from the Department of Otorhinolaryngology, Klinikum Grosshadern, Ludwig Maximilians University of Munich, and Dritter Orden Clinic, Munich-Nymphenburg, Germany. All clinical samples were made fully anonymous. To isolate human primary B cells, T cells were depleted by erythrocyte rosetting using sheep red blood cells and B cells were separated by Ficoll density gradient centrifugation as recommended by the manufacturer (GE Healthcare). The remaining erythrocytes were lysed in red blood cell lysis buffer (155 mM NH_4Cl, 10 mM $KHCO_3$, 0.1 mM EDTA). Cells were co-stained by anti-CD3$^+$ (UCHT1; BD Pharmingen) and anti-CD19$^+$(HIB19; BD Pharmingen) antibodies and analyzed by flow cytometry.

To generate LCLs, primary human B cells were infected with recombinant EBV at a ratio of 1 green Raji unit (GRU) to 10 cells for 48 h and cultivated in medium containing 0.5 μg/ml cyclosporine A for 2 weeks before routine cell culture conditions were applied.

Antibodies, Western blot, immunoprecipitation, and GST-pulldown

Monoclonal antibodies specific for His$_6$ (2F12), EBNA2 (R3), glutathione S transferase (6G9), HA-tag (3F10), BSA (3C5), and LMP1 (1G6) were provided by the antibody facility of the Helmholtz Center Munich. Commercial providers were as follows: GAPDH (Mab374; Merck Millipore), Flag (M2; Sigma-Aldrich), PLK1 (ab17056; Abcam), GFP (7.1 and 13.1; Roche), and a p300-specific serum (C20; Santa Cruz). For immunoprecipitations and Western blotting, the equivalent of 1×10^7 cells was lysed in 500 μl of lysis buffer (1% NP-40, 10 mM Tris–HCl pH 7.4, 3% glycerol, 150 mM

NaCl, 1 mM EDTA) supplemented with cOmplete protease inhibitor and PhoStop phosphatase inhibitor (Roche) incubated for 30 min at 4°C with constant rolling and for 30 min on ice. The lysate was cleared by centrifugation (16,000 *g*, 15 min). 1 μg of purified antibodies or 100 μl of hybridoma supernatants was coupled to Protein A or G beads and added to the cleared lysates, incubated for 2 h at 4°C, and washed with lysis buffer, and the protein was eluted with Laemmeli buffer. For GST-pulldown, antibody-coated beads were replaced by GST fusion protein-coated beads. 20 μg protein of total cell lysates or 5×10^6 cell equivalents of one immunoprecipitation were loaded per lane. Signals on Western blots were detected by enhanced chemiluminescence (GE Healthcare) and exposed to films or Fusion FX (Vilber Lourmat).

Construction of plasmids

All plasmids used in the study were constructed by conventional PCR, restriction digestion, and ligation. Mutated alleles were generated by overlap PCR adapted from the previous protocol (reviewed in Francis *et al*, 2017). In essence, overlap PCR is based on four strategically designed primers. Internally positioned primers must contain complementary sequences to each other, and both of them must contain the mutation of interest, like a substitution, a deletion, or an insertion. The flanking primers might contain restriction enzyme recognition sites to facilitate the cloning of the amplified fragment. Two steps were performed, in the first round of PCRs using the forward primer of the flanking primers with the reverse primer of the internally positioned primers and vice versa, respectively. The resulting amplified short fragments worked as templates when mixed with the flanking primer pairs, which results in amplification of the final long fragment with the desired mutation in the second round of PCR. The second PCR product is digested and inserted into a corresponding vector. For each plasmid used in the study, detailed information about primer pairs, template, and vector is shown in Table EV2.

Expression and purification of His- or GST-tagged proteins

His$_6$-tagged and GST-tagged proteins were expressed in *E. coli* Rosetta (DE3) cells and purified according to manufacturer's instructions using Ni-chelate agarose (Quiagen) or glutathione coupled Sepharose 4B beads (GE Healthcare).

Kinase assay *in vitro*

Purified protein or protein coupled to beads were incubated for 30 min at 37°C with recombinant active Cyclin B/CDK1 (100 ng) or PLK1 (50 ng) in the presence of 1mM normal ATP or plus 0.25 mCi/ml γ-^{32}P labeled ATP in PK buffer (50 mM Tris–HCl, 10 mM MgCl$_2$, 0.1 mM EDTA, 2 mM DTT, 0.01% Brij 35, pH 7.5) in a total reaction volume of 20 μl.

EBV BAC recombineering

All recombinant EBV strains used in this study were generated by a two-step selection protocol using the λ-prophage-based heat-inducible Red recombination system expressed in *E. coli* strain SW105 (Warming *et al*, 2005; Wang *et al*, 2009; Pich *et al*, 2019).

For the first step, a Kan/rpsL expression cassette was flanked by 50 nt EBV sequences of the respective EBNA2 gene locus by PCR using the template p6012. The resulting PCR product was used to insert the Kan/rpsL cassette by homologous recombination into the specific EBV/EBNA2 target site by transformation and kanamycin (30 μg/ml) and chloramphenicol (12.5 μg/ml) selection of SW105 pre-transformed with the recombinant target EBV plasmid. As a second step, a synthetic DNA fragment or PCR product carrying the desired mutation flanked by ˜300 nt of the genomic viral sequence was used to replace the Kan/rpsL cassette by homologous recombination to generate the final mutant EBV plasmid by streptomycin (1 mg/ml) and chloramphenicol (12.5 μg/ml) selection. For each BACmid used in the study, detailed information about primer pairs, template, and vector is shown in Table EV2.

Production of recombinant virus

HEK293 transfectants carrying the recombinant virus plasmid were induced for virus production by co-transfection of 0.5 μg of the plasmids p509 encoding BZLF1 and p2670 encoding BALF4 per one 6-well in 3 ml cell cultures. The supernatants of the transfectants were harvested 3 days post-transfection and passed through a 0.8-μm filter. For quantification of viral titers, 1×10^5 Raji cells were infected with serial dilutions of viral supernatants in 2 ml cultures and the percentage of GFP-positive cells was determined by FACS analysis 3 days post-infection. The concentration of viral stocks was expressed as the number of green Raji units (GRU) (Table 1).

Isothermal titration calorimetry

Experiments were performed on a ITC200 instrument in triplicates and analyzed with the Malvern software. 100 μM PBD was provided in the cell and titrated with 1 mM concentration of wild type (PNTSSPS) or phosphopeptide (PNTSpSPS) with 25 times 1.5 μl injections at 25°C.

Generation and infection of humanized mice

NOD scid $\gamma_c^{-/-}$ (NSG) mice obtained from the Jackson Laboratories were bred and maintained under specific pathogen-free conditions at the Institute of Experimental Immunology, University of Zurich. CD34$^+$ human hematopoietic progenitor cells were isolated from human fetal liver tissue (obtained from Advanced Bioscience Resources) using the CD34 MicroBead Kit (Miltenyi Biotec) following the protocol provided by the manufacturer. Newborn NSG mice (age: 1–5 days) were irradiated with 1 Gy by use of an X-ray source. 1–3×10^5 CD34$^+$ human hematopoietic progenitor cells were injected intrahepatically 5–7 h after irradiation. Reconstitution of mice with human immune system components was investigated 10–12 weeks after engraftment by flow cytometry for the cell surface expression of huCD45 (BV605 or Pacific Blue, clone HI30; BioLegend), huCD3 (PE, clone UCHT1; BV785, clone OKT3; BioLegend), huCD19 (PE-Cy7, clone HIB19; BioLegend) and (PE-Texas Red, Clone SJ25-C1), huCD4 (APC-Cy7, clone RPA-T4; BioLegend), huCD8 (PerCP, clone SK1; BioLegend), huNKp46 (APC, clone 9E2; BD), and HLA-DR (FITC or PE-Cy7 clone L243; BioLegend) on PBMCs. 12–16 weeks after engraftment, humanized mice were infected intraperitoneally with 1x10^5 GRU of EBV wt, EBV S379A, or EBV S457A/T465V. For each

experiment, a different cohort of mice reconstituted with CD34^{+} cells derived from one donor was generated. The animals were ascribed to a distinct experimental group ensuring similar ratios of males to females and similar reconstitution levels and immune cell activation in the peripheral blood. 5 weeks after infection, mice were sacrificed if not necessitated earlier by the regulations of our experimental animal license as a consequence of general health conditions or weight loss over 20%. For analysis of the experiments, only those mice that showed two of the following signs of infection were regarded as infected and included in the analysis: (i) viral loads in spleen, (ii) viral loads in blood at one time-point during the experiment, and (iii) EBNA2^{+} cells in spleen as evaluated by histology. The respective animal protocol (ZH159-17/ZH008-20) was approved by the veterinary office of the canton of Zurich, Switzerland.

Whole blood and spleen preparations for immune phenotyping

Whole blood of mice was collected from the tail vein and prepared for immunophenotyping by lysing erythrocytes with NH_4Cl. Spleens of mice were mashed, subsequently filtered with a 70-μm cell strainer, and afterward mononuclear cells were separated using Ficoll-Paque gradients. Total cell counts were determined from purified mononuclear cell suspensions using a DxH500 Hematology Analyzer (Beckman Coulter). Purified cell suspensions were stained for 30–40 min at 4°C in the dark with a master mix of the respective antibodies followed by a washing step in PBS. The stained cells were analyzed in an LSRFortessa cytometer (BD Biosciences). Flow cytometry data were analyzed using the FlowJo software.

EBV DNA quantification in tissue

Total DNA from splenic tissue and whole blood was extracted using DNeasy Blood & Tissue Kit (QIAGEN) and NucliSENS (bioMérieux),

respectively, according to manufacturer's instructions. Quantitative analysis of EBV DNA in humanized mouse spleens and blood was performed by a TaqMan (Applied Biosystems) real-time PCR as described previously (Berger et al, 2001) with modified primers (5′-CTTCTCAGTCCAGCGCGTTT-3′ and 5′-CAGTGGTCCCCCTCCCTAG A-3′) and the fluorogenic probe (5′-(FAM)-CGTAAGCCAGACAGCA GCCAATTGTCAG-(TAMRA)-3′) for the amplification of a 70-base pair sequence in the conserved BamHI W fragment of EBV. Real-time PCR was run on a ViiA 7 Real-time PCR system or a CFX384 Touch Real-Time PCR Detection System, and samples were analyzed in duplicates.

IgV gene rearrangement sequence analysis

For PCR analysis of rearranged immunoglobulin genes, macroscopically visible tumors were dissected and cryofixated in Tissue Tek® O.C.T.™ (VWR, Cat# SAKU4583) on dry ice.

DNA was isolated from 10 to 20 8-μm frozen tissue sections of biopsies from humanized mice using the PureGene DNA Isolation Kit (Qiagen, Hilden, Germany). PCR was performed with six framework region 1 subgroup-specific primers and a JH primer mix (3′ JH mix) for 35 cycles in six separate reactions, using 300 ng of DNA per reaction. Primer sequences have been published before (Kuppers et al, 2013). PCR products were purified from agarose gels and Sanger sequenced with the IGHV primers used for PCR and the BigDye Sequencing Kit (ABI, Heidelberg, Germany) on an Applied Biosystems 3130 Genetic Analyzer (ABI). Sequences were evaluated with IMGT/V-Quest software (http://www.imgt.org/IMGT_vquest/input).

Mass spectrometry of EBNA2 co-immunoprecipitates

DG75 cells were transfected with a C-terminal HA-tagged EBNA2 (plasmid: pAG155) using electroporation. After 48 h, cells were

Table 1. IgH V gene analysis of B-cell lymphoproliferations.

Mouse	Tissue	EBV	Clonality	VH subgroup or gene[a]	DH gene[b,c]	JH gene[c]	Reading frame[c]
#13	spleen	wt	poly poly poly	VH1 VH3 VH4			
#23	spleen	S379A	poly poly poly	VH1 VH3 VH4			
#23	peritoneum	S379A	mono	VH3-15	DH3-10	JH4	in-frame
#15	spleen	S379A	mono mono	VH2-70 VH1-45	DH3-16 DH6-13	JH4 JH4	in-frame out of frame
#15	peritoneum	S379A	mono mono	VH4-39 VH1-2	DH6-6 n.i.	JH4 JH4	out of frame in-frame
#8	lymph node	S457A/T465V	poly mono	VH1 VH4-39	n.i.	JH4	in-frame
#18[d]	spleen	S457A/T465V	mono poly oligo/poly mono	VH3-30 VH1 VH3 VH1-2	DH6-19 DH2-15	JH6 JH4	in-frame out of frame

[a]If only the VH subgroup is specified, this means that PCR products were obtained for these subgroups (typically for the three largest subgroups VH1, VH3, and VH4), and that a polyclonal composition was revealed upon direct sequencing of these amplicates.
[b]n.i.: D gene sequence was not identified.
[c]Sanger sequencing results obtained from monoclonal tumor specimen.
[d]Specimen was taken from different parts of the spleen.

lysed in NP-40 lysis buffer (1% NP-40, 10 mM Tris–HCl pH 7.4, 3% glycerol, 150 mM NaCl, 1 mM EDTA supplemental with cOmplete protease and PhoStop phosphatase inhibitor). Cell debris was depleted by centrifugation. The cell extract was incubated with protein G beads covalently coupled with an HA-specific antibody. Immunoprecipitates were eluted with Laemmeli buffer.

After reduction and alkylation using DTT and IAA, the proteins were centrifuged on a 30 kDa cutoff filter device and washed thrice with UA buffer (8 M urea in 0.1 M Tris/HCl pH 8.5) and twice with 50 mM ammonium bicarbonate. The proteins were digested for 16 h at 37°C using 1 µg trypsin. After centrifugation (10 min at 14,000 ×*g*), the eluted peptides were acidified with 0.5% trifluoroacetic acid and stored at −20°C.

LC-MS/MS analysis was performed on a LTQ Orbitrap XL mass spectrometer (Thermo Scientific, Waltham, MA, USA) online coupled to an Ultimate 3000 nano-RSLC (Thermo Scientific). Tryptic peptides were automatically loaded on a C18 trap column (300 µm inner diameter (ID) × 5 mm, Acclaim PepMap100 C18, 5 µm, 100 Å, LC Packings) prior to C18 reversed-phase chromatography on the analytical column (Acclaim PepMap C18, 50 µm ID × 250 mm, 2 µm, 100 Å, LC Packings) at 300 nl/min flow rate in a 140-min acetonitrile gradient from 4 to 30% in 0.1% formic acid. Profile precursor spectra from 300 to 1,500 m/z were recorded in the Orbitrap with a maximum injection time of 500 ms. TOP10 fragment spectra of charges 2–7 were recorded in the linear ion trap with a maximum injection time of 100 ms, an isolation window of 2.0 m/z, a normalized collision energy of 35, and a dynamic exclusion of 60 s.

Raw files were analyzed using Progenesis QI for proteomics (version 2.0, Nonlinear Dynamics, part of Waters). Features of charges 2–7 were used, and all MS/MS spectra were exported as mgf file. Peptide searches were performed using Mascot search engine (version 2.5.1) against the Ensembl Human protein database (100158 sequences, 37824871 residues). Search settings were as follows: 10 ppm precursor tolerance, 0.6 Da fragment tolerance, one missed cleavage allowed. Carbamidomethyl on cysteine was set as a fixed modification, deamidation of glutamine and asparagine allowed as variable modification, as well as oxidation of methionine. Applying the percolator algorithm with a cutoff of 13 and $P < 0.05$ resulted in a peptide false discovery rate (FDR) of 1.54%. Search results were reimported in the Progenesis QI software. Proteins were quantified by summing up the abundances of all unique peptides per protein. Resulting protein abundances were used for the calculation of fold changes and statistical values.

Mass spectrometry on purified EBNA2 phosphorylated by PLK1 *in vitro*

EBNA2 and GST-fused EBNA2 proteins, purified from bacteria, were subjected to PLK1 kinase assays. 50 µg EBNA2 or 130 µg GST-fused EBNA2 protein was incubate in 1× PK buffer (NEB, 50 mM Tris–HCl, 10 mM MgCl₂, 0.1 mM EDTA, 2 mM DTT, 0.01% Brij 35, pH 7.5), 1.25 mM ATP in the presence or absence of 250 ng active PLK1 (SignalChem) at 37°C for 1 h. All reactions were carried out in a total volume of 20 µl and then were quenched with 5 µl 5× Laemmli sample buffer.

Proteins were separated by SDS–PAGE and stained with Coomassie Colloidal Blue. Bands corresponding to EBNA2 full

length (86 kD) or GST-EBNA2 C-terminal fragment (28 kD) were sliced out from the gel lane, and proteins were then reduced, alkylated, and digested with either trypsin or GluC (Roche), as previously described (Shevchenko *et al*, 1996).

Dried peptides were reconstituted in 0.1% FA/2% ACN and subjected to MS analysis using a Dionex Ultimate 3000 UHPLC⁺ system coupled to a Fusion Lumos Tribrid mass spectrometer (Thermo Fisher). Peptides were delivered to a trap column (75 µm × 2 cm, packed in-house with 5 µm Reprosil C18 resin; Dr. Maisch) and washed using 0.1% FA at a flow rate of 5 µl/min for 10 min. Subsequently, peptides were transferred to an analytical column (75 µm × 45 cm, packed in-house with 3 µm Reprosil C18 resin, Dr. Maisch) applying a flow rate of 300 nl/min. Peptides were chromatographically separated using a 50-min linear gradient from 4 to 32% solvent B (0.1% FA, 5% DMSO in ACN) in solvent A (0.1% FA in 5% DMSO). The mass spectrometer was operated in data-dependent mode, automatically switching between MS and MS/MS. Full-scan MS spectra (from m/z 360–1,500) were acquired in the Orbitrap with a resolution of 60,000 at m/z 200, using an automatic gain control (AGC) target value of 5e5 charges and maximum injection time (maxIT) of 10 ms. The 10 most intense ions within the survey scan were selected for HCD fragmentation with normalized collision energy set to 28%.

Isolation window was set to 1.7 Th, and MS/MS spectra were acquired in the Orbitrap with a resolution of 15,000 at m/z 200, using an AGC target value of 2e5, and a maxIT of 75 ms. Dynamic exclusion was set to 20 s.

Peptide and protein identification was performed using MaxQuant (version 1.5.3.30) with its built in search engine Andromeda (Cox & Mann, 2008). Spectra were searched against a SwissProt database, either the *Spodoptera frugiperda* (OX 7108 - 26,502 sequences) or *Escherichia coli* (UP000002032 – 4,156 sequences), supplemented with the EBNA2 protein sequence. Enzyme specificity was set to Trypsin/P or GluC accordingly, and the search included cysteine carbamidomethylation as a fixed modification, protein N-term acetylation, oxidation of methionine, and phosphorylation of serine, threonine, tyrosine residue (STY) as variable modifications. Up to two and three missed cleavage sites were allowed for trypsin and GluC, respectively. Precursor tolerance was set to 4.5 ppm (after MS1 feature re-calibration) and fragment ion tolerance to 20 ppm. The match between runs feature was enabled. Peptide identification was further filtered for a minimum Andromeda score of 20 or 40, for unmodified and modified (phosphorylated) sequences, respectively. A site localization probability of at least 0.75 was used as the threshold for confident localization (Vizcaíno *et al*, 2013, 2016).

Cell proliferation assay

Human adenoid primary B cells were stained with CellTrace Violet according to the manufacturer's instructions (Thermo Fisher Scientific). Proliferation of CD19⁺ B cells was monitored by flow cytometry using BD Fortessa, and the data were analyzed using the FlowJo software (Version 10.5.3).

Dual-luciferase assay

5×10^6 DG75 cells were electroporated with 1.5 µg EBNA2 expression plasmids and the luciferase construct 1.5 µg pGa981.6

(Minoguchi *et al*, 1997) carrying a multimerized CBF1 binding site to measure EBNA2 activity and 0.2 µg Renilla luciferase expression plasmid. 24 h post electroporation, cells were washed, pelleted, and lysed in 100 µl lysis buffer for 30 min on ice. Cell extracts were tested by the dual-luciferase assay according to the manufacturer's instructions (Promega).

Data availability

Phosphorylation of EBNA2 by PLK1: The mass spectrometry proteomic data have been deposited in the ProteomeXchange Consortium via the PRIDE partner repository http://proteomecentral.proteomexchange.org/cgi/GetDataset with the dataset identifier PXD022970 (Vizcaíno *et al*, 2013, 2016).

Expanded View for this article is available online.

Author contributions

XZ, MS, CM, RK, and BKe conceptualized the study; AMo, PG, and SMH involved in formal analysis and data curation; XZ, PS, MR, KS, and CM contributed to methodology; BKe and CM involved in funding acquisition; XZ, PS, AMo, PG, AMu, ST, CK-R, SB, and RK investigated the study; WH, MR, MS, CM, KS, BKu, and CM provided resources; WH, RK, MS, CM, and BKe supervised the study; XZ, PS, AMo, and BKe visualized the study; XZ and BKe wrote—original draft; XZ, MS, CM, PG, PS, AMo, BKe, and RK wrote—review & editing.

Conflict of interest

The authors declare that they have no conflict of interest.

References

Ando K, Ozaki T, Yamamoto H, Furuya K, Hosoda M, Hayashi S, Fukuzawa M, Nakagawara A (2004) Polo-like kinase 1 (Plk1) inhibits p53 function by physical interaction and phosphorylation. *J Biol Chem* 279: 25549–25561

Baluapuri A, Wolf E, Eilers M (2020) Target gene-independent functions of MYC oncoproteins. *Nat Rev Mol Cell Biol* 21: 255–267

Barr FA, Silljé HHW, Nigg EA (2004) Polo-like kinases and the orchestration of cell division. *Nat Rev Mol Cell Biol* 5: 429–440

Ben-Bassat H, Goldblum N, Mitrani S, Goldblum T, Yoffey JM, Cohen MM, Bentwich Z, Ramot B, Klein E, Klein G (1977) Establishment in continuous culture of a new type of lymphocyte from a "Burkitt like" malignant lymphoma (line D.G.-75). *Int J Cancer* 19: 27–33

Berger C, Day P, Meier G, Zingg W, Bossart W, Nadal D (2001) Dynamics of Epstein-Barr virus DNA levels in serum during EBV-associated disease. *J Med Virol* 64: 505–512

Caduff N, McHugh D, Murer A, Rämer P, Raykova A, Landtwing V, Rieble L, Keller CW, Prummer M, Hoffmann L *et al* (2020) Immunosuppressive FK506 treatment leads to more frequent EBV-associated lymphoproliferative disease in humanized mice. *PLoS Pathog* 16: e1008477

de Carcer G (2019) The mitotic cancer target polo-like kinase 1: oncogene or tumor suppressor? *Genes* 10: 208

Chabot PR, Raiola L, Lussier-Price M, Morse T, Arseneault G, Archambault J, Omichinski JG (2014) Structural and functional characterization of a complex between the acidic transactivation domain of EBNA2 and the Tfb1/p62 subunit of TFIIH. *PLoS Pathog* 10: e1004042

Chatterjee B, Deng Y, Holler A, Nunez N, Azzi T, Vanoaica LD, Müller A, Zdimerova H, Antsiferova O, Zbinden A *et al* (2019) CD8+ T cells retain protective functions despite sustained inhibitory receptor expression during Epstein-Barr virus infection in vivo. *PLOS Pathog* 15: e1007748

Cheng K-Y, Lowe ED, Sinclair J, Nigg EA, Johnson LN (2003) The crystal structure of the human polo-like kinase-1 polo box domain and its phospho-peptide complex. *EMBO J* 22: 5757–5768

Cohen JI (1992) A region of herpes simplex virus VP16 can substitute for a transforming domain of Epstein-Barr virus nuclear protein 2. *Proc Natl Acad Sci USA* 89: 8030–8034

Cohen JI, Kieff E (1991) An Epstein-Barr virus nuclear protein 2 domain essential for transformation is a direct transcriptional activator. *J Virol* 65: 5880–5885

Cohen JI, Wang F, Kieff E (1991) Epstein-Barr virus nuclear protein 2 mutations define essential domains for transformation and transactivation. *J Virol* 65: 2545–2554

Cox J, Mann M (2008) MaxQuant enables high peptide identification rates, individualized p.p.b.-range mass accuracies and proteome-wide protein quantification. *Nat Biotechnol* 26: 1367–1372

Delecluse HJ, Hilsendegen T, Pich D, Zeidler R, Hammerschmidt W (1998) Propagation and recovery of intact, infectious Epstein-Barr virus from prokaryotic to human cells. *Proc Natl Acad Sci USA* 95: 8245–8250

Edgar RC (2004) MUSCLE: a multiple sequence alignment method with reduced time and space complexity. *BMC Bioinformatics* 5: 113

Elia AEH, Cantley LC, Yaffe MB (2003a) Proteomic screen finds pSer/pThr-binding domain localizing Plk1 to mitotic substrates. *Science* 299: 1228–1231

Elia AEH, Rellos P, Haire LF, Chao JW, Ivins FJ, Hoepker K, Mohammad D, Cantley LC, Smerdon SJ, Yaffe MB (2003b) The molecular basis for phosphodependent substrate targeting and regulation of Plks by the Polo-box domain. *Cell* 115: 83–95

Farrell CJ, Lee JM, Shin EC, Cebrat M, Cole PA, Hayward SD (2004) Inhibition of Epstein-Barr virus-induced growth proliferation by a nuclear antigen EBNA2-TAT peptide. *Proc Natl Acad Sci USA* 101: 4625–4630

Farrell PJ (2019) Epstein-Barr virus and cancer. *Annu Rev Pathol* 14: 29–53

Francis MS, Amer AAA, Milton DL, Costa TRD (2017) Site-directed mutagenesis and its application in studying the interactions of T3S components. In: *Type 3 secretion systems: Methods and protocols*, Nilles ML, Condry DLJ (eds). pp. 11–31. New York, NY: Springer New York

Friberg A, Thumann S, Hennig J, Zou P, Nossner E, Ling PD, Sattler M, Kempkes B (2015) The EBNA-2 N-terminal transactivation domain folds into a dimeric structure required for target gene activation. *PLoS Pathog* 11: e1004910

Gheghiani L, Loew D, Lombard B, Mansfeld J, Gavet O (2017) PLK1 activation in late G2 sets up commitment to mitosis. *Cell Rep* 19: 2060–2073

Glaser LV, Rieger S, Thumann S, Beer S, Kuklik-Roos C, Martin DE, Maier KC, Harth-Hertle ML, Grüning B, Backofen R *et al* (2017) EBF1 binds to EBNA2

and promotes the assembly of EBNA2 chromatin complexes in B cells. *PLoS Pathog* 13: e1006664

Harter MR, Liu CD, Shen CL, Gonzalez-Hurtado E, Zhang ZM, Xu M, Martinez E, Peng CW, Song J (2016) BS69/ZMYND11 C-terminal domains bind and inhibit EBNA2. *PLoS Pathog* 12: e1005414

Henkel T, Ling PD, Hayward SD, Peterson MG (1994) Mediation of Epstein-Barr virus EBNA2 transactivation by recombination signal-binding protein J kappa. *Science* 265: 92−95

Hsieh JJ, Hayward SD (1995) Masking of the CBF1/RBPJ kappa transcriptional repression domain by Epstein-Barr virus EBNA2. *Science* 268: 560−563

Kaiser C, Laux G, Eick D, Jochner N, Bornkamm GW, Kempkes B (1999) The proto-oncogene c-myc is a direct target gene of Epstein-Barr virus nuclear antigen 2. *J Virol* 73: 4481−4484

Kempkes B, Ling PD (2015) EBNA2 and Its coactivator EBNA-LP. *Curr Top Microbiol Immunol* 391: 35−59

Koida N, Ozaki T, Yamamoto H, Ono S, Koda T, Ando K, Okoshi R, Kamijo T, Omura K, Nakagawara A (2008) Inhibitory role of Plk1 in the regulation of p73-dependent apoptosis through physical interaction and phosphorylation. *J Biol Chem* 283: 8555−8563

Kuppers R, Schneider M, Hansmann ML (2013) Laser-based microdissection of single cells from tissue sections and PCR analysis of rearranged immunoglobulin genes from isolated normal and malignant human B cells. *Methods Mol Biol* 971: 49−63

Kuppers R, Zhao M, Rajewsky K, Hansmann ML (1993) Detection of clonal B cell populations in paraffin-embedded tissues by polymerase chain reaction. *Am J Pathol* 143: 230−239

Kwiatkowski B, Chen SY, Schubach WH (2004) CKII site in Epstein-Barr virus nuclear protein 2 controls binding to hSNF5/Ini1 and is important for growth transformation. *J Virol* 78: 6067−6072

Lee KH, Hwang J-A, Kim S-O, Kim JH, Shin SC, Kim EE, Lee KS, Rhee K, Jeon BH, Bang JK et al (2018) Phosphorylation of human enhancer filamentation 1 (HEF1) stimulates interaction with Polo-like kinase 1 leading to HEF1 localization to focal adhesions. *J Biol Chem* 293: 847−862

Lee KS, Park JE, Kang YH, Kim TS, Bang JK (2014) Mechanisms underlying Plk1 polo-box domain-mediated biological processes and their physiological significance. *Mol Cells* 37: 286−294

Ling PD, Hayward SD (1995) Contribution of conserved amino acids in mediating the interaction between EBNA2 and CBF1/RBPJk. *J Virol* 69: 1944−1950

Liu Z, Sun Q, Wang X (2017) PLK1, a potential target for cancer therapy. *Transl Oncol* 10: 22−32

Longnecker RM, Kieff E, Cohen JI (2013) Epstein-Barr virus. In: *Fields virology*, Knipe DM, Howley PM, Cohen JI, Griffin DE, Lamb RA, Martin MA, Racianello VR, Roizman B (eds.), Vol. 2, 6th edn, pp 1898−1959. Philadelphia, PA: Lippincott Williams and Wilkins

Lowery DM, Lim D, Yaffe MB (2005) Structure and function of Polo-like kinases. *Oncogene* 24: 248−259

Lu F, Chen HS, Kossenkov AV, DeWispeleare K, Won KJ, Lieberman PM (2016) EBNA2 drives formation of new chromosome binding sites and target genes for B-cell master regulatory transcription factors RBP-jkappa and EBF1. *PLoS Pathog* 12: e1005339

Marceau AH, Brison CM, Nerli S, Arsenault HE, McShan AC, Chen E, Lee HW, Benanti JA, Sgourakis NG, Rubin SM (2019) An order-to-disorder structural switch activates the FoxM1 transcription factor. *Elife* 8: e46131

Martin BT, Strebhardt K (2006) Polo-like kinase 1: target and regulator of transcriptional control. *Cell Cycle* 5: 2881−2885

Minoguchi S, Taniguchi Y, Kato H, Okazaki T, Strobl LJ, Zimber-Strobl U, Bornkamm GW, Honjo T (1997) RBP-L, a transcription factor related to RBP-Jkappa. *Mol Cell Biol* 17: 2679−2687

Mrozek-Gorska P, Buschle A, Pich D, Schwarzmayr T, Fechtner R, Scialdone A, Hammerschmidt W (2019) Epstein-Barr virus reprograms human B lymphocytes immediately in the prelatent phase of infection. *Proc Natl Acad Sci USA* 116: 16046−16055

Munz C (2019) Latency and lytic replication in Epstein-Barr virus-associated oncogenesis. *Nat Rev Microbiol* 17: 691−700

Nakajima H, Toyoshima-Morimoto F, Taniguchi E, Nishida E (2003) Identification of a consensus motif for Plk (Polo-like kinase) phosphorylation reveals Myt1 as a Plk1 substrate. *J Biol Chem* 278: 25277−25280

Pavlovsky AG, Liu X, Faehnle CR, Potente N, Viola RE (2012) Structural characterization of inhibitors with selectivity against members of a homologous enzyme family. *Chem Biol Drug Des* 79: 128−136

Pich D, Mrozek-Gorska P, Bouvet M, Sugimoto A, Akidil E, Grundhoff A, Hamperl S, Ling PD, Hammerschmidt W (2019) First days in the life of naive human B lymphocytes infected with Epstein-Barr Virus. *MBio* https://doi.org/10.1128/mbio.01723-19

Ponnusamy R, Khatri R, Correia PB, Wood CD, Mancini EJ, Farrell PJ, West MJ (2019) Increased association between Epstein-Barr virus EBNA2 from type 2 strains and the transcriptional repressor BS69 restricts EBNA2 activity. *PLoS Pathog* 15: e1007458

Pulvertaft JV (1964) Cytology of Burkitt's tumour (African Lymphoma). *Lancet* 39: 238−240

Raab M, Sanhaji M, Matthess Y, Hörlin A, Lorenz I, Dötsch C, Habbe N, Waidmann O, Kurunci-Csacsko E, Firestein R et al (2018) PLK1 has tumor-suppressive potential in APC-truncated colon cancer cells. *Nat Commun* 9: 1106

Rajewsky K (1996) Clonal selection and learning in the antibody system. *Nature* 381: 751−758

Ren Y, Bi C, Zhao X, Lwin T, Wang C, Yuan JI, Silva AS, Shah BD, Fang B, Li T et al (2018) PLK1 stabilizes a MYC-dependent kinase network in aggressive B cell lymphomas. *J Clin Invest* 128: 5517−5530

Rodel F, Zhou S, Gyorffy B, Raab M, Sanhaji M, Mandal R, Martin D, Becker S, Strebhardt K (2020) The prognostic relevance of the proliferation markers Ki-67 and Plk1 in early-stage ovarian cancer patients with serous, low-grade carcinoma based on mRNA and protein expression. *Front Oncol* 10: 558932

Rosenblum D, Gutkin A, Kedmi R, Ramishetti S, Veiga N, Jacobi AM, Schubert MS, Friedmann-Morvinski D, Cohen ZR, Behlke MA et al (2020) CRISPR-Cas9 genome editing using targeted lipid nanoparticles for cancer therapy. *Sci Adv* 6: eabc9450

Shannon-Lowe C, Rickinson A (2019) The global landscape of EBV-associated tumors. *Front Oncol* 9: 713

Shevchenko A, Wilm M, Vorm O, Mann M (1996) Mass spectrometric sequencing of proteins silver-stained polyacrylamide gels. *Anal Chem* 68: 850−858

Shultz LD, Saito Y, Najima Y, Tanaka S, Ochi T, Tomizawa M, Doi T, Sone A, Suzuki N, Fujiwara H et al (2010) Generation of functional human T-cell subsets with HLA-restricted immune responses in HLA class I expressing NOD/SCID/IL2r gamma(null) humanized mice. *Proc Natl Acad Sci USA* 107: 13022−13027

Śledź P, Lang S, Stubbs CJ, Abell C (2012) High-throughput interrogation of ligand binding mode using a fluorescence-based assay. *Angew Chem Int Ed Engl* 51: 7680−7683

Strebhardt K (2010) Multifaceted polo-like kinases: drug targets and antitargets for cancer therapy. *Nat Rev Drug Discov* 9: 643–660

Strebhardt K, Ullrich A (2006) Targeting polo-like kinase 1 for cancer therapy. *Nat Rev Cancer* 6: 321–330

Strowig T, Gurer C, Ploss A, Liu Y-F, Arrey F, Sashihara J, Koo G, Rice CM, Young JW, Chadburn A *et al* (2009) Priming of protective T cell responses against virus-induced tumors in mice with human immune system components. *J Exp Med* 206: 1423–1434

Thorley-Lawson DA (2001) Epstein-Barr virus: exploiting the immune system. *Nat Rev Immunol* 1: 75–82

Thorley-Lawson DA, Gross A (2004) Persistence of the Epstein-Barr virus and the origins of associated lymphomas. *N Engl J Med* 350: 1328–1337

Tong X, Drapkin R, Reinberg D, Kieff E (1995a) The 62- and 80-kDa subunits of transcription factor IIH mediate the interaction with Epstein-Barr virus nuclear protein 2. *Proc Natl Acad Sci USA* 92: 3259–3263

Tong X, Drapkin R, Yalamanchili R, Mosialos G, Kieff E (1995b) The Epstein-Barr virus nuclear protein 2 acidic domain forms a complex with a novel cellular coactivator that can interact with TFIIE. *Mol Cell Biol* 15: 4735–4744

Tong X, Wang F, Thut CJ, Kieff E (1995c) The Epstein-Barr virus nuclear protein 2 acidic domain can interact with TFIIB, TAF40, and RPA70 but not with TATA-binding protein. *J Virol* 69: 585–588

Vizcaíno JA, Côté RG, Csordas A, Dianes JA, Fabregat A, Foster JM, Griss J, Alpi E, Birim M, Contell J *et al* (2013) The proteomics identifications (PRIDE) database and associated tools: status in 2013. *Nucleic Acids Res* 41: D1063–1069

Vizcaíno J, Csordas A, del-Toro N, Dianes JA, Griss J, Lavidas I, Mayer G, Perez-Riverol Y, Reisinger F, Ternent T *et al* (2016) 2016 update of the PRIDE database and its related tools. *Nucleic Acids Res* 44: 11033

Wang L, Grossman SR, Kieff E (2000) Epstein-Barr virus nuclear protein 2 interacts with p300, CBP, and PCAF histone acetyltransferases in activation of the LMP1 promoter. *Proc Natl Acad Sci USA* 97: 430–435

Wang S, Zhao Y, Leiby M, Zhu J (2009) A new positive/negative selection scheme for precise BAC recombineering. *Mol Biotechnol* 42: 110–116

Warming S, Costantino N, Court DL, Jenkins NA, Copeland NG (2005) Simple and highly efficient BAC recombineering using galK selection. *Nucleic Acids Res* 33: e36

Watanabe N, Arai H, Iwasaki J, Shiina M, Ogata K, Hunter T, Osada H (2005) Cyclin-dependent kinase (CDK) phosphorylation destabilizes somatic Wee1 via multiple pathways. *Proc Natl Acad Sci USA* 102: 11663–11668

West MJ (2017) Chromatin reorganisation in Epstein-Barr virus-infected cells and its role in cancer development. *Curr Opin Virol* 26: 149–155

Wolf G, Elez R, Doermer A, Holtrich U, Ackermann H, Stutte HJ, Altmannsberger H-M, Rübsamen-Waigmann H, Strebhardt K (1997) Prognostic significance of polo-like kinase (PLK) expression in non-small cell lung cancer. *Oncogene* 14: 543–549

Yuan C, Wang L, Zhou L, Fu Z (2014) The function of FOXO1 in the late phases of the cell cycle is suppressed by PLK1-mediated phosphorylation. *Cell Cycle* 13: 807–819

Yuan J, Eckerdt F, Bereiter-Hahn J, Kurunci-Csacsko E, Kaufmann M, Strebhardt K (2002) Cooperative phosphorylation including the activity of polo-like kinase 1 regulates the subcellular localization of cyclin B1. *Oncogene* 21: 8282–8292

Yuan J, Horlin A, Hock B, Stutte HJ, Rubsamen-Waigmann H, Strebhardt K (1997) Polo-like kinase, a novel marker for cellular proliferation. *Am J Pathol* 150: 1165–1172

Yue W, Davenport MG, Shackelford J, Pagano JS (2004) Mitosis-specific hyperphosphorylation of Epstein-Barr virus nuclear antigen 2 suppresses its function. *J Virol* 78: 3542–3552

Yue W, Gershburg E, Pagano JS (2005) Hyperphosphorylation of EBNA2 by Epstein-Barr virus protein kinase suppresses transactivation of the LMP1 promoter. *J Virol* 79: 5880–5885

Yue W, Shackelford J, Pagano JS (2006) cdc2/cyclin B1-dependent phosphorylation of EBNA2 at Ser243 regulates its function in mitosis. *J Virol* 80: 2045–2050

Yun S-M, Moulaei T, Lim D, Bang JK, Park J-E, Shenoy SR, Liu FA, Kang YH, Liao C, Soung N-K *et al* (2009) Structural and functional analyses of minimal phosphopeptides targeting the polo-box domain of polo-like kinase 1. *Nat Struct Mol Biol* 16: 876–882

Zdimerova H, Murer A, Engelmann C, Raykova A, Deng Y, Gujer C, Rühl J, McHugh D, Caduff N, Naghavian R *et al* (2021) Attenuated immune control of Epstein-Barr virus in humanized mice is associated with the multiple sclerosis risk factor HLA-DR15. *Eur J Immunol* 51: 64–75